Publication VII

N. Lebedeva and P. Kuivalainen, Spin-dependent current through a ferromagnetic resonant tunnelling quantum well, Physica Status Solidi (b), vol.242, pp. 1660-1678, 2005.

Reprinted with permission from N. Lebedeva and P. Kuivalainen, Physica Status Solidi (b), vol. 242, pp.1660-1678, (2005). Copyright 2005, WILEY-VCH Verlag.

physica status solidi b

phys. stat. sol. (b) **242**, No. 8, 1660–1678 (2005) / **DOI** 10.1002/pssb.200440045

Spin-dependent current through a ferromagnetic resonant tunnelling quantum well

N. Lebedeva and **P. Kuivalainen***

Electron Physics Laboratory, Department of Electrical and Communications Engineering, Helsinki University of Technology, P.O. Box 3500, 02015 HUT, Finland

Received 16 December 2004, revised 4 April 2005, accepted 19 April 2005
Published online 7 June 2005

PACS 72.10.–d, 72.20.Dp, 72.25.Mk, 73.63.Hs

We study the nonequilibrium quantum transport through a ferromagnetic quantum well (FQW) coupled to two nonmagnetic leads. A formal expression for the spin-polarized current is derived with the Keldysh nonequilibrium-Green-function technique. Then the retarded Green function for the FQW, which is needed in the general expression for the transmission coefficient $T(E)$, is calculated by using Zubarev's double-time-Green-function technique. The derived expression for $T(E)$ includes, e.g., the shift and the life-time broadening of the electronic states inside the FQW due to the tunnelling processes and the strong exchange interaction between the charge carrier spins and the localized spins of the magnetic electrons. Numerical results are presented for a simple FQW model structure consisting of a diluted III–V ferromagnetic semiconductor between the insulating barriers. A single resonant level inside the FQW is coupled to the nonmagnetic leads by tunnelling and to the ferromagnetic subsystem by the exchange interaction. Novel effects predicted by the model are discussed, such as the broadening of the resonant level due to the spin-disorder scattering in a 2D-hole gas and the large spontaneous spin-splitting of the resonant level in a ferromagnetic phase transition. These effects are seen in the calculated $T(E)$ and the spin current through the FQW, which show strong temperature and magnetic field dependences at temperatures close to the Curie temperature.

© 2005 WILEY-VCH Verlag GmbH & Co. KGaA, Weinheim

1 Introduction

Due to the recent advances in semiconductor technology and nanoelectronics, the control and manipulation of the spin degree of freedom in electronic devices is becoming increasingly important [1–4]. For instance, in semiconductor nanostructures and mesoscopic devices, such as quantum dots, the spin–spin interaction between the charge carriers can no longer be neglected as in the conventional semiconductor devices. During the last few years, however, the major factor affecting the rapid progress and emergence of the semiconductor spintronics has been the discovery of ferromagnetism in the conventional III–V compound semiconductors like InAs [5] and GaAs [6], when heavily doped with manganese. These new ferromagnetic semiconductors are fully compatible with the existing III–V device technology, which offers an excellent opportunity to study the spin-dependent charge transport in well-defined ferromagnetic device structures. Some simple devices such as ferromagnetic pn-junctions and light emitting diodes [7–9], GaMnAs/AlAs superlattices [10], and GaMnAs/AlGaAs trilayer [11] and resonant tunnelling structures [12] have already been made of the epitaxial GaMnAs films. The introduction of the magnetically sensitive elements to the device structure can greatly enhance the functionality of the new fer-

* Corresponding author: e-mail: pekka.kuivalainen@hut.fi

© 2005 WILEY-VCH Verlag GmbH & Co. KGaA, Weinheim

romagnetic semiconductor devices. The ferromagnetism remains even in 5–7 nm thin GaMnAs layers [13], which allows, e.g., a fabrication of ferromagnetic quantum wells.

Resonant tunnelling of electrons or holes through nonmagnetic semiconductor double-barrier heterostructures has been studied extensively both theoretically and experimentally since the pioneering work of Tsu and Esaki [14]. The resonant tunnelling is a powerful tool for the spectroscopy of the electronic states inside the quantum wells, and the resonant tunnelling diodes (RTDs) have a lot of interesting applications in the high-speed electronics [see ref. 15 and references therein]. The first magnetic RTD was made by Bremer et al. [16], who investigated paramagnetic/antiferromagnetic ErAs quantum well in the GaAs based AlAs/ErAs/AlAs structure. They observed, e.g., a large spin splitting of the electronic states in the quantum well under magnetic fields. The first ferromagnetic quantum well (FQW) was fabricated by Haury et al. [17] by using CdMnTe technology. However, the Curie temperature T_C in the magnetic layer was very low, $T_C = 2\,\mathrm{K}$, and the electrical transport properties were not studied. A III–V compound semiconductor RTD with a ferromagnetic emitter was investigated experimentally by Ohno et al. [12] by using heavily Mn-doped GaAs as an emitter material. The Curie temperature was 70 K in the emitter region, but the quantum well was nonmagnetic. The spin–splitting of the valence band in the emitter region was observed below T_C in the I–V characteristics.

The modelling of the nonmagnetic RTDs is now a mature field, either when using semiclassical approach [14, 18] or more advanced theoretical methods for the quantum transport in solids [19–21]. On the other hand, only a few papers have been published on the theory of the ferromagnetic RTDs [22–25] or other ferromagnetic semiconductor devices [26–30]. We have studied recently the modelling of the basic ferromagnetic devices such as pn-diodes and bipolar transistors by using a semiclassical drift-diffusion transport theory [26]. The same problem has been treated independently by Fabian et al. [27–30], also by using a semiclassical approach. More advanced transport theory has been developed for the RTD with a ferromagnetic emitter by Nonoyama and Inoue [22]. They developed a recursive Green-function method based on the Keldysh formalism and they could explain novel effects in the experimental I–V characteristics. The detailed valence band structure of GaAs was taken into account by Petukhov et al. [23], when they calculated the spin–dependent resonant tunnelling through a nonmagnetic quantum well separated from two ferromagnetic electrodes by thin insulating barriers. Their model predicts a strongly enhanced tunnelling magnetoresistance for certain quantum well widths.

The first work, where the ferromagnetic quantum well RTD has been studied theoretically, was published by Petukhov et al. [24] a few years ago. Their approach was based on the $\boldsymbol{k}\cdot\boldsymbol{p}$ perturbation theory, and they considered in detail the resonant tunnelling of holes in a GaMnAs FQW by taking into account the real valence band structure of GaAs. However, the transport model was semiclassical and it did not include scattering effects. Recently the same group [25] considered theoretically spin–dependent interband resonant tunnelling in magnetic heterostructures with type-II broken-gap band alignment found in double-barrier InAs/AlSb/$Ga_{1-x}Mn_xSb$ diodes.

In the present paper we discuss quantum transport theory for spin current in a ferromagnetic resonant tunnelling quantum well. Our approach is based on the quantum statistical formulation originally developed by Meir and Wingreen [19] and later applied to various nonmagnetic mesoscopic structures (see Ref. 20 and references therein). A nice feature in the chosen formalism for our purposes is a straightforward inclusion of the strong spin–spin (exchange) interaction in the current expression via the advanced and retarded Green functions for the FQW. These Green functions are derived by using Zubarev's double-time-Green-function technique [31]. This approach allows us to take into account simultaneously both the spin disorder scattering and tunnelling effects in the calculation of the spin current through the FQW.

2 Model Hamiltonian

Let us consider a ferromagnetic quantum well (FQW) shown schematically in Fig. 1(a). Here the FQW is coupled to two nonmagnetic metallic leads by tunneling processes through thin insulating barriers on the left and right sides of the FQW. The magnetic subsystem consists of the localized magnetic electrons,

© 2005 WILEY-VCH Verlag GmbH & Co. KGaA, Weinheim

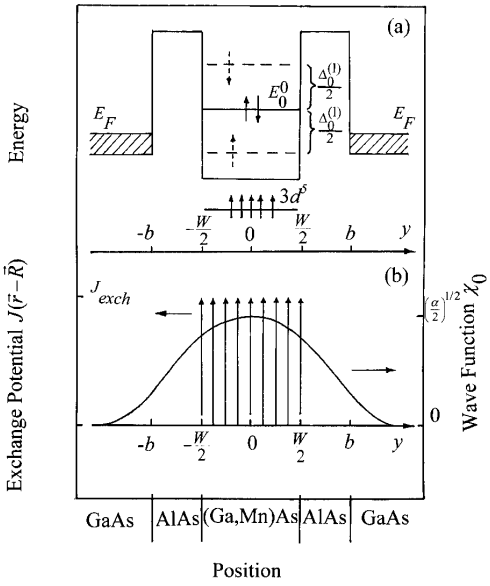

Fig. 1 (a) Schematic drawing of a ferromagnetic resonant-tunneling structure under zero bias. The quantum well of width W has a quasibound state at energy E_0^0 (only the lowest state is shown). The dashed lines inside the well describe the spin-polarized states, when the spins of the magnetic atoms order ferromagnetically (e.g. the five localized spins/atom at the level 3d in the case of Mn doped GaAs). $\Delta_0^{(1)}$ is the band splitting parameter given by (10). (b) Contact-type exchange potential $J(\boldsymbol{r}-\boldsymbol{R}) \sim \delta(\boldsymbol{r}-\boldsymbol{R})$ inside the well region $-W/2 < y < W/2$. The solid curve shows the wave function vs. position in the well region for the lowest bound state $\chi_0(y)$.

e.g., the five 3d electrons/atom in the case of Mn-doped III–V compound semiconductors. The spin operator for the total spin of the magnetic electrons in a magnetic atom at a lattice site $\boldsymbol{R}$ is denoted by $\boldsymbol{S}_{\boldsymbol{R}}$. Then a Heisenberg-type Hamiltonian for the magnetic subsystem inside the FQW is given by

$$H_m = -\sum_{\boldsymbol{R},\boldsymbol{R}'} I(\boldsymbol{R},\boldsymbol{R}')\,\boldsymbol{S}_{\boldsymbol{R}} \cdot \boldsymbol{S}_{\boldsymbol{R}'} - g_L \mu_B B \sum_{\boldsymbol{R}} S_{\boldsymbol{R}}^Z \tag{1}$$

where $I(\boldsymbol{R},\boldsymbol{R}')$ is the ferromagnetic coupling constant between the localized spins $\boldsymbol{S}_{\boldsymbol{R}}$ and $\boldsymbol{S}_{\boldsymbol{R}'}$ of the magnetic atoms at the lattice sites $\boldsymbol{R}$ and $\boldsymbol{R}'$, respectively. The last term in (1) gives the Zeeman energy when an external magnetic field $\boldsymbol{B}$ has been applied in the z-direction, i.e., in the plane of the quantum well. The average spin polarization can now be calculated by using the Hamiltonian (1) [32]:

$$\left\langle S_{\boldsymbol{R}}^Z \right\rangle = \frac{\mathrm{Tr}(\mathrm{e}^{-\beta H_m} S_{\boldsymbol{R}}^Z)}{\mathrm{Tr}(\mathrm{e}^{-\beta H_m})} \tag{2}$$

where $\beta = 1/k_B T$. From (1) and (2) one gets a self-consistent equation for $\left\langle S_{\boldsymbol{R}}^Z \right\rangle$, e.g., in the mean-field approximation (see below).

We assume that the unperturbed eigenstates and – values $\phi_{n\boldsymbol{k}\sigma}$ and $E_{n\boldsymbol{k}\sigma}^0$, respectively, are known in the case of the noninteracting Hamiltonian $H_{\mathrm{el}}^{\mathrm{QW}} = -\hbar^2\nabla^2/2m^* + V_{\mathrm{QW}}(y)$ for the quantum well, where $V_{\mathrm{QW}}(y)$ is the potential of the well shown in Fig. 1(a):

$$\phi_{n\boldsymbol{k}\sigma} = \phi_{n\boldsymbol{k}}(\boldsymbol{r})\,|\sigma\rangle = \frac{1}{\sqrt{L_x L_z}}\,\mathrm{e}^{i(k_x x + k_z z)}\,\chi_n(y)\,|\sigma\rangle\,, \tag{3}$$

$$E_{n\boldsymbol{k}\sigma}^0 = E_n^0 + \frac{\hbar^2(k_x^2 + k_z^2)}{2m^*}\,. \tag{4}$$

Here L_x and L_z are the dimensions of the well in x- and z-directions, respectively. χ_n and E_n^0 denote the eigenstates and -values for the y-dependent part of the Hamiltonian $H_{\mathrm{el}}^{\mathrm{QW}}$ (in Fig. 1(a) only the lowest

© 2005 WILEY-VCH Verlag GmbH & Co. KGaA, Weinheim

level E_0^0 is shown). The states $|\sigma\rangle$ are the eigenstates of the charge carrier spin operator $\boldsymbol{s} = \sigma/2$, where σ is the Pauli spin matrix. For simplicity we assume that the charge carriers in a one-band spin–polarized model can be described by a single isotropic effective mass m^*.

The magnetic and electronic subsystems of the FQW are coupled by the spin–spin (exchange) interaction between the charge carrier spins and the spins of the localized magnetic electrons, which is given by

$$H_{\text{exch}} = -\sum_{\boldsymbol{R}} J(\boldsymbol{r} - \boldsymbol{R})\, \boldsymbol{s} \cdot \boldsymbol{S}_{\boldsymbol{R}} \ . \tag{5}$$

Here $J(\boldsymbol{r} - \boldsymbol{R})$ is the exchange potential, which is assumed to be of the contact-potential type as shown in Fig. 1 (b), and it is given by

$$J(\boldsymbol{r} - \boldsymbol{R}) = J_{\text{exch}}\, \Omega_{\text{QW}}\, \delta(\boldsymbol{r} - \boldsymbol{R})\, \theta(y + W/2)\, \theta(W/2 - y) \ . \tag{6}$$

Here J_{exch} is the exchange interaction parameter, which may be as large as 1–3 eV in the III–V diluted magnetic semiconductors [3]. $\Omega_{QW} = (L_x L_z W / N_x N_y N_z)$ is the volume of the unit cell in the well region having the width W, and N_α is the number of lattice points in the direction $\alpha = x, y, z$. The Heaviside step function θ limits the potential (6) within the well region $-W/2 < y < W/2$ (see Fig. 1(b)). When calculating the effects of the perturbation (5) on the electronic states and on the carrier life-time inside the FQW, it is convenient to insert the identity $\boldsymbol{S}_{\boldsymbol{R}} = \boldsymbol{S}_{\boldsymbol{R}} + \langle \boldsymbol{S}_{\boldsymbol{R}} \rangle - \langle \boldsymbol{S}_{\boldsymbol{R}} \rangle$ into (5). Then we can re-express the Hamiltonians $H_{\text{el}}^{\text{QW}}$ and H_{exch} as follows

$$H_{\text{el}}^{\text{FQW}}(\sigma) = -\frac{\hbar^2 \nabla^2}{2m^*} + V_{\text{QW}}(y) - \frac{(\delta_{\sigma\uparrow} - \delta_{\sigma\downarrow})}{2} \sum_{\boldsymbol{R}} J(\boldsymbol{r} - \boldsymbol{R}) \left\langle S_{\boldsymbol{R}}^z \right\rangle \ , \tag{7}$$

$$H_{\text{exch}} = -\sum_{\boldsymbol{R}} J(\boldsymbol{r} - \boldsymbol{R})\, \boldsymbol{s} \cdot \left(\boldsymbol{S}_{\boldsymbol{R}} - \left\langle S_{\boldsymbol{R}}^z \right\rangle \right) \ . \tag{8}$$

The last term in (7) can be interpreted as a perturbation potential, when the first order energy correction for the spin–polarized electronic states in the FQW is calculated:

$$E_{n\boldsymbol{k}\sigma}^{(1)} = E_{n\boldsymbol{k}\sigma}^0 - \frac{(\delta_{\sigma\uparrow} - \delta_{\sigma\downarrow})}{2} \sum_{\boldsymbol{R}} \langle \phi_{n\boldsymbol{k}\sigma} | J(\boldsymbol{r} - \boldsymbol{R}) | \phi_{n\boldsymbol{k}\sigma} \rangle \left\langle S_{\boldsymbol{R}}^z \right\rangle \equiv E_{n\boldsymbol{k}\sigma}^0 - \frac{\Delta_n^{(1)} (\delta_{\sigma\uparrow} - \delta_{\sigma\downarrow})}{2} \ . \tag{9}$$

Here $\Delta_n^{(1)}$ is the band splitting parameter describing the energy difference between the spin-up and spin-down electronic states in the FQW. By using the eigenstates (3) and the exchange potential (6), $\Delta_{n\sigma}^{(1)}$ can be calculated, and it is given by

$$\Delta_n^{(1)} = -x \left\langle S^z \right\rangle J_{\text{exch}}\, \Omega_{\text{QW}} \sum_{\boldsymbol{R}} \mathrm{e}^{i\boldsymbol{k}\cdot\boldsymbol{R}}\, \chi_n^*(R_y)\, \chi_n(R_y) = -x \left\langle S^z \right\rangle J_{\text{exch}}\, F_n(W) \tag{10}$$

where x is the mole fraction of the magnetic atoms. The function $F_n(W)$, which was obtained in (10) by using the 2-dimensional lattice summation rule $\sum_{\boldsymbol{R}} \mathrm{e}^{i\boldsymbol{k}\cdot\boldsymbol{R}} = N_x N_z \delta_{\boldsymbol{k},0}$, is given by

$$F_n(W) = \sum_{|R_y| \le W/2} \frac{W \chi_n^*(R_y)\, \chi_n(R_y)}{N_y} \tag{11}$$

and it measures how large fraction of the charge density $\rho(y) = \sum_n \chi_n^*(y) \chi_n(y)$ lies inside the quantum well: As shown schematically in Fig. 1(b) for the ground state wave function $\chi_0(y)$, due to the tunneling processes a part of the wave function may extend outside the well, and consequently $F_n < 1$, which reduces the effect of the exchange potential on the band splitting (10). In the 3-dimensional case, where

© 2005 WILEY-VCH Verlag GmbH & Co. KGaA, Weinheim

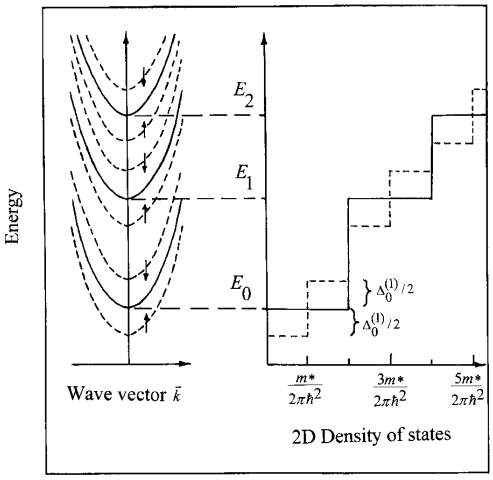

Fig. 2 Spin-polarized energy band structure and density of states for a 2D carrier system inside the FQW.

$W \to \infty$ and $\chi \to \exp(ik_y R_y)/\sqrt{L_y}$, the function $F_n \to 1$, and we get from (10) our previous 3D result for the band splitting [33]. Based on Eqs. (4) and (9) we can present the spin-polarized band structure and density of states for a 2D charge carrier system in the FQW, as shown schematically in Fig. 2.

The calculation of the Green functions below requires the presentation of the Hamiltonians (7) and (8) in the second quantization formalism. Therefore, by using the wave functions (3), we can define the following field operators for the charge carriers inside the FQW:

$$\hat{\psi}_\sigma(\boldsymbol{r}) = \sum_{nk} \phi_{nk\sigma}(\boldsymbol{r})\, a_{nk\sigma} \ , \tag{12}$$

$$\hat{\psi}^\dagger_\sigma(\boldsymbol{r}) = \sum_{nk} \phi^*_{nk\sigma}(\boldsymbol{r})\, a^\dagger_{nk\sigma} \tag{13}$$

where $a^\dagger_{nk\sigma}$ and $a_{nk\sigma}$ are the creation and annihilation operators, respectively, for a charge carrier in the state $|\phi_{nk\sigma}\rangle$. Then the Hamiltonians (7) and (8) are given by

$$\hat{H}^{\mathrm{FQW}}_{\mathrm{el}} = \int \mathrm{d}^3\boldsymbol{r}\hat{\psi}^\dagger_\sigma(\boldsymbol{r})\, H^{\mathrm{FQW}}_{\mathrm{el}}(\boldsymbol{r})\, \hat{\psi}_\sigma(\boldsymbol{r}) = \sum_{nk\sigma} E^{(1)}_{nk\sigma} a^\dagger_{nk\sigma} a_{nk\sigma} \tag{14}$$

and

$$\begin{aligned}\hat{H}_{\mathrm{exch}} = \sum_\sigma \int \mathrm{d}^3\boldsymbol{r}\hat{\psi}^\dagger_\sigma(\boldsymbol{r})\, H_{\mathrm{exch}}(\boldsymbol{r})\, \hat{\psi}_\sigma(\boldsymbol{r}) \ &= -\sum_{\substack{nk,n'k' \\ \sigma,\sigma',\boldsymbol{R} \\ |R_y|\le W/2}} \left\langle \phi^*_{nk\sigma} \middle| J(\boldsymbol{r}-\boldsymbol{R})\, \boldsymbol{s} \middle| \phi_{n'k'\sigma'} \right\rangle (\boldsymbol{S}_{\boldsymbol{R}} - \langle \boldsymbol{S}_{\boldsymbol{R}} \rangle)\, a^\dagger_{nk\sigma} a_{n'k'\sigma'} \\ &= -\left(\frac{J_{\mathrm{exch}} \Omega_{\mathrm{QW}}}{2} \right) \sum_{\substack{nk,nk',\boldsymbol{R} \\ |R_y|\le W/2}} \phi^*_{nk}(\boldsymbol{R})\, \phi_{n'k'}(\boldsymbol{R}) \\ &\times \left[S^+_{\boldsymbol{R}} a^\dagger_{nk\downarrow} a_{n'k'\uparrow} + S^-_{\boldsymbol{R}} a^\dagger_{nk\uparrow} a_{n'k'\downarrow} + \left(S^z_{\boldsymbol{R}} - \langle S^z_{\boldsymbol{R}} \rangle \right) \left(a^\dagger_{nk\uparrow} a_{n'k'\uparrow} - a^\dagger_{nk\downarrow} a_{n'k'\downarrow} \right) \right] .\end{aligned} \tag{15}$$

© 2005 WILEY-VCH Verlag GmbH & Co. KGaA, Weinheim

Here the spin raising and spin lowering operators are defined as usual by $S_{\boldsymbol{R}}^{+} = S_{\boldsymbol{R}}^{x} + iS_{\boldsymbol{R}}^{y}$ and $S_{\boldsymbol{R}}^{-} = S_{\boldsymbol{R}}^{x} - iS_{\boldsymbol{R}}^{y}$, respectively. The first two terms in (15) describe the spin-flip scattering processes of the charge carriers, and the last two terms are responsible for the scattering without the spin-flip transitions.

The nonmagnetic leads connected to the insulating barriers (see Fig. 1(a)) are described by the following Hamiltonian:

$$\hat{H}_{\mathrm{el}}^{c} = \sum_{k\in L,\,\sigma} E_{k\sigma}^{0} b_{k\sigma}^{\dagger} b_{k\sigma} + \sum_{k\in R,\,\sigma} E_{k\sigma}^{0} b_{k\sigma}^{\dagger} b_{k\sigma} \tag{16}$$

where $b_{k\sigma}^{\dagger}$ and $b_{k\sigma}$ are the creation and destruction operators for a charge carrier at an energy level $E_{k\sigma}^{0}$ either in the left (L) or right (R) contact. Finally, we need an operator that describes the tunnelling processes between the leads and the FQW. It is given by [18, 31]

$$\hat{H}_{T} = \sum_{\substack{k\in L\\ nk'\sigma}} \langle \boldsymbol{k}\sigma | V_{L}(\boldsymbol{r}) | n\boldsymbol{k}'\sigma \rangle\, b_{k\sigma}^{\dagger} a_{nk'\sigma} + \sum_{\substack{k\in L\\ nk'\sigma}} \langle n\boldsymbol{k}'\sigma | V_{L}(\boldsymbol{r}) | \boldsymbol{k}\sigma \rangle\, a_{nk'\sigma}^{\dagger} b_{k\sigma}$$

$$+ \sum_{\substack{k\in R\\ nk'\sigma}} \langle \boldsymbol{k}\sigma | V_{R}(\boldsymbol{r}) | n\boldsymbol{k}'\sigma \rangle\, b_{k\sigma}^{\dagger} a_{nk'\sigma} + \sum_{\substack{k\in R\\ nk'\sigma}} \langle n\boldsymbol{k}'\sigma | V_{R}(\boldsymbol{r}) | \boldsymbol{k}\sigma \rangle\, a_{nk'\sigma}^{\dagger} b_{k\sigma} \tag{17}$$

where $V_{L(R)}(\boldsymbol{r})$ is the barrier potential on the left (right) side of the well region.

To summarize, we can write our final model Hamiltonian for the FQW as

$$\hat{H}_{\mathrm{tot}} = \hat{H}_{\mathrm{el}}^{\mathrm{FQW}} + \hat{H}_{\mathrm{el}}^{c} + H_{m} + \hat{H}_{\mathrm{exch}} + \hat{H}_{T} \tag{18}$$

where all the Hamiltonians, excluding the magnetic one H_m, are expressed in the second quantization formalism, as discussed above. The Hamiltonian (18) leads to a difficult transport problem, and therefore, in order to keep the treatment at a reasonable level, we have neglected many important interactions such as coulombic interaction between the charge carriers and the ionized impurities, electron–phonon interaction, and spin–orbit coupling. The chosen formalism would allow the inclusion of these interactions, but the equations of motion for the Green functions would become unnecessarily complicated. We are interested mainly in the effect of ferromagnetism on the carrier transport through a FQW, and this is included in (18).

3 Retarded Green function for the FQW

The electronic and magnetic properties of the FQW described by the Hamiltonian (18) can be calculated by means of Zubarev's double-time-Green-function technique [31], where the retarded Green function constructed by using operators A and B is defined by

$$G_{r}(t,t') = \langle\langle A(t); B(t')\rangle\rangle_{r} = -i\theta(t-t')\left\langle A(t)\,B(t') + B(t')\,A(t)\right\rangle. \tag{19}$$

Here the brackets $\langle \ldots \rangle$ denote the thermal average, and $A(t)$ and $B(t)$ are the operators in the Heisenberg picture. By using the Heisenberg equation of motion for the operators, it can be shown [31] that the time-Fourier-transformed Green function $\langle\langle A; B\rangle\rangle_{\hbar\omega}$ satisfies the following equation of motion:

$$\hbar\omega\langle\langle A; B\rangle\rangle_{\hbar\omega} = \left\langle [A, B]_{\eta}\right\rangle + \langle\langle (AH_{\mathrm{tot}} - H_{\mathrm{tot}}A); B\rangle\rangle_{\hbar\omega} \tag{20}$$

© 2005 WILEY-VCH Verlag GmbH & Co. KGaA, Weinheim

where the index $\eta = +1$ or -1 denotes the commutator or anticommutator, respectively, and $H_{\rm tot}$ is the total Hamiltonian of the system. Now we can write the equation of motion for the FQW propagator $G_r(n\boldsymbol{k}\sigma; n''\boldsymbol{k}''\sigma'') = \langle\langle a_{n\boldsymbol{k}\sigma}; a^{\dagger}_{n''\boldsymbol{k}''\sigma''}\rangle\rangle$ with $\eta = -1$ by inserting the Hamiltonian (18) into (20), which yields

$$\hbar\omega G_r(n\boldsymbol{k}\sigma; n''\boldsymbol{k}''\sigma'') = \delta_{nn''}\delta_{\boldsymbol{k}\boldsymbol{k}''}\delta_{\sigma\sigma''} + E^{(1)}_{n\boldsymbol{k}\sigma} G_r(n\boldsymbol{k}\sigma; n''\boldsymbol{k}''\sigma'') + \sum_{\boldsymbol{p}\in L}\langle n\boldsymbol{k}\sigma|V_L(\boldsymbol{r})|\boldsymbol{p}\sigma\rangle\langle\langle b_{\boldsymbol{p}\sigma}; a^{\dagger}_{n''\boldsymbol{k}''\sigma''}\rangle\rangle$$

$$+\sum_{\boldsymbol{p}\in R}\langle n\boldsymbol{k}\sigma|V_R(\boldsymbol{r})|\boldsymbol{p}\sigma\rangle\langle\langle b_{\boldsymbol{p}\sigma}; a^{\dagger}_{n''\boldsymbol{k}''\sigma''}\rangle\rangle - \left(\frac{J_{\rm exch}\Omega_{\rm QW}}{2}\right)\sum_{\substack{n'\boldsymbol{p}\boldsymbol{R}\\ |R_y|\le W/2}}\phi^{*}_{n\boldsymbol{k}}(\boldsymbol{R})\,\phi_{n'\boldsymbol{p}}(\boldsymbol{R})$$

$$\times\Big[\langle\langle\left(S^{z}_{\boldsymbol{R}} - \langle S^{z}_{\boldsymbol{R}}\rangle\right)a_{n'\boldsymbol{p}\sigma}; a^{\dagger}_{n''\boldsymbol{k}''\sigma}\rangle\rangle(\delta_{\sigma\uparrow} - \delta_{\sigma\downarrow})$$

$$+\langle\langle S^{-}_{\boldsymbol{R}}a_{n'\boldsymbol{p}\downarrow}; a^{\dagger}_{n''\boldsymbol{k}''\sigma''}\rangle\rangle\delta_{\sigma\uparrow} + \langle\langle S^{+}_{\boldsymbol{R}}a_{n'\boldsymbol{p}\uparrow}; a^{\dagger}_{n''\boldsymbol{k}''\sigma''}\rangle\rangle\delta_{\sigma\downarrow}\Big]. \tag{21}$$

Similarly for the Green function $\langle\langle b_{\boldsymbol{p}\sigma}; a^{\dagger}_{n''\boldsymbol{k}''\sigma''}\rangle\rangle$ in (21) we get the equation of motion by inserting (16) and (17) into (20), which yields

$$\hbar\omega\langle\langle b_{\boldsymbol{p}\sigma}; a^{\dagger}_{n''\boldsymbol{k}''\sigma''}\rangle\rangle = E^{0}_{\boldsymbol{p}\sigma}\langle\langle b_{\boldsymbol{p}\sigma}; a^{\dagger}_{n''\boldsymbol{k}''\sigma''}\rangle\rangle + \sum_{n\boldsymbol{k}'}\langle\boldsymbol{p}\sigma|V_{L(R)}|n\boldsymbol{k}'\sigma\rangle\langle\langle a_{n\boldsymbol{k}'\sigma}; a^{\dagger}_{n''\boldsymbol{k}''\sigma''}\rangle\rangle$$

or

$$\langle\langle b_{\boldsymbol{p}\sigma}; a^{\dagger}_{n''\boldsymbol{k}''\sigma''}\rangle\rangle = \sum_{n\boldsymbol{k}'}\frac{\langle\boldsymbol{p}\sigma|V_{L(R)}|n\boldsymbol{k}'\sigma\rangle}{\hbar\omega - E^{0}_{\boldsymbol{p}\sigma}}\langle\langle a_{n\boldsymbol{k}'\sigma}; a^{\dagger}_{n''\boldsymbol{k}''\sigma}\rangle\rangle \tag{22}$$

where $\boldsymbol{p}\in L$ (or R). A more difficult task is to derive and solve the equations of motion for the higher order Green functions $\langle\langle\left(S^{\beta}_{\boldsymbol{R}} - \langle S^{\beta}_{\boldsymbol{R}}\rangle\right)a_{n\boldsymbol{p}\sigma}; a^{\dagger}_{n''\boldsymbol{k}''\sigma''}\rangle\rangle$, with $\beta = z, +,$ or -, appearing in (21). As an example, let us consider the equation of motion for the Green function $\langle\langle S^{-}_{\boldsymbol{R}}a_{n\boldsymbol{p}\sigma}; a^{\dagger}_{n''\boldsymbol{k}''\sigma''}\rangle\rangle$. It is obtainable by inserting (14), (15) and (17) into (20), which yields

$$\hbar\omega\langle\langle S^{-}_{\boldsymbol{R}}a_{n'\boldsymbol{p}\downarrow}; a^{\dagger}_{n''\boldsymbol{k}''\sigma''}\rangle\rangle = E^{(1)}_{n'\boldsymbol{p}\downarrow}\langle\langle S^{-}_{\boldsymbol{R}}a_{n'\boldsymbol{p}\downarrow}; a^{\dagger}_{n''\boldsymbol{k}''\sigma''}\rangle\rangle$$

$$+\frac{J_{\rm exch}\Omega_{QW}}{2}\sum_{\substack{\tilde{k}''',n''',\boldsymbol{R}'\\ |R'_y|\le W/2}}\langle S^{-}_{\boldsymbol{R}}S^{+}_{\boldsymbol{R}'}\rangle\phi^{*}_{n'\boldsymbol{p}}(\boldsymbol{R})\,\phi_{n'''\boldsymbol{k}'''}(\boldsymbol{R}')\langle\langle a_{n'''\boldsymbol{k}'''\uparrow}; a^{\dagger}_{n''\boldsymbol{k}''\sigma''}\rangle\rangle$$

$$+\sum_{\boldsymbol{k}\in L}\langle n'\boldsymbol{p}\downarrow|V_L(\boldsymbol{r})|\boldsymbol{k}\downarrow\rangle\langle\langle S^{-}_{\boldsymbol{R}}b_{\boldsymbol{k}\downarrow}; a^{\dagger}_{n''\boldsymbol{k}''\sigma''}\rangle\rangle$$

$$+\sum_{\boldsymbol{k}\in R}\langle n'\boldsymbol{p}\downarrow|V_R(\boldsymbol{r})|\boldsymbol{k}\downarrow\rangle\langle\langle S^{-}_{\boldsymbol{R}}b_{\boldsymbol{k}\downarrow}; a^{\dagger}_{n''\boldsymbol{k}''\sigma''}\rangle\rangle. \tag{23}$$

Here we have decoupled the higher order Green functions by replacing the products of the spin operators by their thermal averages

$$\langle\langle S^{-}_{\boldsymbol{R}}S^{+}_{\boldsymbol{R}}a_{n\boldsymbol{k}\sigma}; a^{\dagger}_{n''\boldsymbol{k}''\sigma''}\rangle\rangle \approx \langle S^{-}_{\boldsymbol{R}}S^{+}_{\boldsymbol{R}}\rangle\langle\langle a_{n\boldsymbol{k}\sigma}; a^{\dagger}_{n''\boldsymbol{k}''\sigma''}\rangle\rangle.$$

By using our previous result (22) we can derive immediately the solution for the equation of motion for the Green function $\langle\langle S^{-}_{\boldsymbol{R}}b_{\boldsymbol{k}\downarrow}; a^{\dagger}_{n''\boldsymbol{k}''\sigma''}\rangle\rangle$ appearing in (23):

$$\langle\langle S^{-}_{\boldsymbol{R}}b_{\boldsymbol{k}\downarrow}; a^{\dagger}_{n''\boldsymbol{k}''\sigma''}\rangle\rangle = \sum_{n\boldsymbol{k}'}\left[\frac{\langle\boldsymbol{k}\downarrow|V_L(\boldsymbol{r})|n'\boldsymbol{k}'\downarrow\rangle}{\hbar\omega - E^{0}_{\boldsymbol{k}\downarrow}} + \frac{\langle\boldsymbol{k}\downarrow|V_R(\boldsymbol{r})|n'\boldsymbol{k}'\downarrow\rangle}{\hbar\omega - E^{0}_{\boldsymbol{k}\downarrow}}\right]\langle\langle S^{-}_{\boldsymbol{R}}a_{n\boldsymbol{k}'\downarrow}; a^{\dagger}_{n''\boldsymbol{k}''\sigma''}\rangle\rangle. \tag{24}$$

© 2005 WILEY-VCH Verlag GmbH & Co. KGaA, Weinheim

Now, inserting (24) back into (23) we get a closed equation for the Green function $\langle\langle S_{\boldsymbol{R}}^{-} a_{n'\boldsymbol{p}\downarrow}; a_{n''\boldsymbol{k}''\sigma''}^{\dagger}\rangle\rangle$, and it has the following solution:

$$\langle\langle S_{\boldsymbol{R}}^{-} a_{n'\boldsymbol{p}\downarrow}; a_{n''\boldsymbol{k}''\sigma''}^{\dagger}\rangle\rangle = \frac{J_{\mathrm{exch}}\Omega_{\mathrm{QW}}}{2} \sum_{\substack{\boldsymbol{k}''',n''',\boldsymbol{R}' \\ |R_z'|\le W/2}} \frac{\langle S_{\boldsymbol{R}}^{-} S_{\boldsymbol{R}'}^{+}\rangle \phi_{n'\boldsymbol{p}}^{*}(\boldsymbol{R})\,\phi_{n'''\boldsymbol{k}'''}(\boldsymbol{R}')}{\hbar\omega - E_{n'\boldsymbol{p}\downarrow}^{(1)} - \Sigma_{\Gamma}(n'\boldsymbol{p}\downarrow)} \langle\langle a_{n'''\boldsymbol{k}'''\uparrow}; a_{n''\boldsymbol{k}''\sigma''}^{\dagger}\rangle\rangle \tag{25}$$

where the self-energy for the tunnelling processes is given by

$$\begin{aligned}\Sigma_{\Gamma}(n'\boldsymbol{p}\sigma) &= \sum_{\boldsymbol{k}\in L} \frac{|\langle \boldsymbol{k}\sigma|\, V_L(\boldsymbol{r})\,|n'\boldsymbol{p}\sigma\rangle|^2}{\hbar\omega - E_{\boldsymbol{k}\sigma}^{0}} + \sum_{\boldsymbol{k}\in R} \frac{|\langle \boldsymbol{k}\sigma|\, V_R(\boldsymbol{r})\,|n'\boldsymbol{p}\sigma\rangle|^2}{\hbar\omega - E_{\boldsymbol{k}\sigma}^{0}} \\ &= \Sigma_{\Gamma}^{\mathrm{Re}}(n'\boldsymbol{p}\sigma) - i\frac{\Gamma(n'\boldsymbol{p}\sigma)}{2}\end{aligned} \tag{26}$$

with

$$\begin{aligned}\Gamma(n'\boldsymbol{p}\sigma) &= 2\pi \sum_{\boldsymbol{k}\in L} |\langle \boldsymbol{k}\sigma|\, V_L(\boldsymbol{r})\,|n'\boldsymbol{p}\sigma\rangle|^2\, \delta(\hbar\omega - E_{\boldsymbol{k}\sigma}^{0}) + 2\pi \sum_{\boldsymbol{k}\in R} |\langle \boldsymbol{k}\sigma|\, V_R(\boldsymbol{r})\,|n'\boldsymbol{p}\sigma\rangle|^2\, \delta(\hbar\omega - E_{\boldsymbol{k}\sigma}^{0}) \\ &= \Gamma_{\sigma}^{L} + \Gamma_{\sigma}^{R}\end{aligned} \tag{27}$$

and

$$\Sigma_{\Gamma}^{\mathrm{Re}} = \int \frac{\mathrm{d}E'}{2\pi} \frac{\Gamma(E')}{(E - E')} \tag{28}$$

is the Hilbert transform of the coupling parameter Γ.

In the same way the equations of motion for the other higher order Green functions $\langle\langle \left(S_{\boldsymbol{R}}^{\beta} - \langle S_{\boldsymbol{R}}^{\beta}\rangle\right) a_{n\boldsymbol{p}\sigma}; a_{n''\boldsymbol{k}''\sigma''}^{\dagger}\rangle\rangle$ with $\beta = z$ and + can be derived. The solutions are similar to (25), when the spin correlation function $\langle S_{\boldsymbol{R}}^{-} S_{\boldsymbol{R}'}^{+}\rangle$ in (25) is replaced by the functions $\langle\langle \left(S_{\boldsymbol{R}}^{z} - \langle S_{\boldsymbol{R}}^{z}\rangle\right)\left(S_{\boldsymbol{R}'}^{z} - \langle S_{\boldsymbol{R}'}^{z}\rangle\right)\rangle\rangle$ and $\langle S_{\boldsymbol{R}}^{+} S_{\boldsymbol{R}'}^{-}\rangle$ for $\beta = z$ and +, respectively. Finally, we can insert (25) and the solutions for the other higher order Green functions (including (22)) into (21), and we get a closed equation for the FQW propagator G_r:

$$\begin{aligned}&[\hbar\omega - E_{n\boldsymbol{k}\sigma}^{(1)} - \Sigma_{\Gamma}(n\boldsymbol{k}\sigma)]\, G_r(n\boldsymbol{k}\sigma; n''\boldsymbol{k}''\sigma'') \\ &= \delta_{nn''}\delta_{\boldsymbol{k}\boldsymbol{k}''}\delta_{\sigma\sigma''} + \frac{J_{\mathrm{exch}}^{2}\Omega_{\mathrm{QW}}^{2}}{4} \sum_{\substack{n'\boldsymbol{p}\boldsymbol{R} \\ n'''\boldsymbol{k}'\boldsymbol{R}'}} \phi_{n\boldsymbol{k}'}^{*}(\boldsymbol{R})\,\phi_{n'\boldsymbol{p}}(\boldsymbol{R})\,\phi_{n'\boldsymbol{p}}^{*}(\boldsymbol{R}')\,\phi_{n'''\boldsymbol{k}'}(\boldsymbol{R}') \\ &\times \left\{ \frac{\langle\langle \left(S_{\boldsymbol{R}}^{z} - \langle S_{\boldsymbol{R}}^{z}\rangle\right)\left(S_{\boldsymbol{R}'}^{z} - \langle S_{\boldsymbol{R}'}^{z}\rangle\right)\rangle\rangle}{\hbar\omega - E_{n'\boldsymbol{p}\sigma}^{(1)} - \Sigma_{\Gamma}(n'\boldsymbol{p}\sigma)} + \frac{\langle S_{\boldsymbol{R}}^{-} S_{\boldsymbol{R}'}^{+}\rangle \delta_{\sigma\uparrow}}{\hbar\omega - E_{n'\boldsymbol{p}\downarrow}^{(1)} - \Sigma_{\Gamma}(n'\boldsymbol{p}\downarrow)} + \frac{\langle S_{\boldsymbol{R}}^{+} S_{\boldsymbol{R}'}^{-}\rangle \delta_{\sigma\downarrow}}{\hbar\omega - E_{n'\boldsymbol{p}\uparrow}^{(1)} - \Sigma_{\Gamma}(n'\boldsymbol{p}\uparrow)} \right\} \\ &\times G_r(n'\boldsymbol{k}'\sigma; n''\boldsymbol{k}''\sigma'')\,.\end{aligned} \tag{29}$$

By defining the first order Green function $G_{n\boldsymbol{k}\sigma}^{(1)} = [\hbar\omega - E_{n\boldsymbol{k}\sigma}^{(1)} - \Sigma_{\Gamma}(n\boldsymbol{k}\sigma)]^{-1}$ we can write (29) formally as a Dyson equation:

$$G_r = G^{(1)} + G^{(1)} \Sigma_{\mathrm{SD}}^{2\mathrm{D}}\, G_r \tag{30}$$

where the self-energy related to the exchange interaction is given by

$$\begin{aligned}\Sigma_{\mathrm{SD}}^{2\mathrm{D}}(E_{n\boldsymbol{k}\sigma}) &= \frac{J_{\mathrm{exch}}^{2}\Omega_{\mathrm{QW}}^{2}}{4} \sum_{\substack{n'\boldsymbol{p}\boldsymbol{R} \\ n'''\boldsymbol{k}'\boldsymbol{R}'}} \phi_{n\boldsymbol{k}}^{*}(\boldsymbol{R})\,\phi_{n'\boldsymbol{p}}(\boldsymbol{R})\,\phi_{n'\boldsymbol{p}}^{*}(\boldsymbol{R}')\,\phi_{n'''\boldsymbol{k}'}(\boldsymbol{R}') \\ &\times \left\{ \frac{C^{zz}(\boldsymbol{R},\boldsymbol{R}')}{E_{n\boldsymbol{k}\sigma} - E_{n'\boldsymbol{p}\sigma}^{(1)} - \Sigma_{\Gamma}(n'\boldsymbol{p}\sigma)} + \frac{C^{xx}(\boldsymbol{R},\boldsymbol{R}')\,\delta_{\sigma\uparrow}}{E_{n\boldsymbol{k}\sigma} - E_{n'\boldsymbol{p}\downarrow}^{(1)} - \Sigma_{\Gamma}(n'\boldsymbol{p}\downarrow)} + \frac{C^{yy}(\boldsymbol{R},\boldsymbol{R}')\,\delta_{\sigma\downarrow}}{E_{n\boldsymbol{k}\sigma} - E_{n'\boldsymbol{p}\uparrow}^{(1)} - \Sigma_{\Gamma}(n'\boldsymbol{p}\uparrow)} \right\}.\end{aligned} \tag{31}$$

© 2005 WILEY-VCH Verlag GmbH & Co. KGaA, Weinheim

Here the spin correlation functions are defined as

$$C^{zz}(\boldsymbol{R},\boldsymbol{R'}) = \left\langle \left(S^z_{\boldsymbol{R}} - \left\langle S^z_{\boldsymbol{R}} \right\rangle\right)\left(S^z_{\boldsymbol{R'}} - \left\langle S^z_{\boldsymbol{R'}} \right\rangle\right)\right\rangle ,$$

$$C^{xx}(\boldsymbol{R},\boldsymbol{R'}) = \left\langle S^-_{\boldsymbol{R}} S^+_{\boldsymbol{R'}} \right\rangle , \tag{32}$$

$$C^{yy}(\boldsymbol{R},\boldsymbol{R'}) = \left\langle S^+_{\boldsymbol{R}} S^-_{\boldsymbol{R'}} \right\rangle .$$

The self-energy (31) is the main result of the present work: Via the spin correlation functions $C^{\alpha\alpha}$ and the tunnelling self-energy Σ_Γ, the Eq. (31) includes both the spin fluctuations and the tunneling effects in the FQW, and thereby allows us to study, e.g., the effect of the spin disorder (SD) scattering on the resonant tunnelling through the FQW structures.

In the 3D case, where no tunnelling effects are present ($\Sigma_\Gamma = 0$) and the electronic states in the band can be described by the plane waves, $\phi_k(\boldsymbol{r}) = V^{-1/2}\exp(i\boldsymbol{k}\cdot\boldsymbol{r})$, the self-energy (31) reduces to our previous result [33] for the bulk magnetic semiconductors:

$$\Sigma^{\mathrm{3D}}_{\mathrm{SD}}(E^{(1)}_{k\sigma}) = \frac{J^2_{\mathrm{exch}}}{4N}\sum_{\boldsymbol{q}}\left[\frac{C^{zz}(\boldsymbol{q})}{E^{(1)}_{k\sigma} - E^{(1)}_{k-q,\sigma}} + \frac{C^{xx}(\boldsymbol{q})\,\delta_{\sigma\uparrow}}{E^{(1)}_{k\sigma} - E^{(1)}_{k-q,\downarrow}} + \frac{C^{yy}(\boldsymbol{q})\,\delta_{\sigma\downarrow}}{E^{(1)}_{k\sigma} - E^{(1)}_{k-q,\uparrow}}\right] \tag{33}$$

where

$$C^{\alpha\alpha}(\boldsymbol{q}) = \sum_{\boldsymbol{R}} \mathrm{e}^{-i\boldsymbol{q}\cdot\boldsymbol{R}} C^{\alpha\alpha}(\boldsymbol{R},0) \tag{34}$$

with $\alpha = x, y, z$ is the Fourier transform of the spin correlation functions (32).

4 Spin-dependent currents and the Keldysh Green functions

Originally the formal quantum transport theory for the dc current in nonmagnetic resonant tunnelling systems was developed by Meir and Wingreen [19] based on Keldysh Green functions. Later the same formalism was extended to time-dependent cases by Jauho et al. [20, 21]. An advantage of this method is that one needs only the single particle retarded Green function $G_r(E)$ for the interacting central region in order to calculate the dc current. Since the derivation of the dc current formula has been treated in detail elsewhere [19–21], we here only briefly outline the main points of the calculation and then, for the first time, apply the results to the FQW.

The dc current from the left contact through the left barrier to the FQW shown in Fig. 1(a) can be calculated from the time evolution of the occupation number operator $\hat{N}^\sigma_L = \sum_{k\in L} b^\dagger_{k\sigma} b_{k\sigma}$:

$$J^\sigma_L = -e\left\langle \frac{\partial \hat{N}^\sigma_L}{\partial t}\right\rangle = \frac{-ie}{\hbar}\left\langle \left[\hat{H}_{\mathrm{tot}}, \hat{N}_L\right]\right\rangle \tag{35}$$

where $\hat{H}_{\mathrm{tot}}$ is given in (18). Since $\hat{H}^{\mathrm{FQW}}_{\mathrm{el}}$, H_m and $\hat{H}_{\mathrm{exch}}$ commute with $\hat{N}^\sigma_L$, we get

$$J^\sigma_L = \frac{ie}{\hbar}\sum_{n,\boldsymbol{k},\boldsymbol{k'}\in L}\left[\langle n\boldsymbol{k}\sigma|V_L(\boldsymbol{r})|\boldsymbol{k'}\sigma\rangle\, G^<_{n\boldsymbol{k}\boldsymbol{k'}\sigma} - \langle \boldsymbol{k'}\sigma|V_L(\boldsymbol{r})|n\boldsymbol{k}\sigma\rangle\, G^<_{\boldsymbol{k'}n\boldsymbol{k}\sigma}\right] \tag{36}$$

where we have defined the 'lesser' Green functions as

$$G^<_{n\boldsymbol{k}\boldsymbol{k'}\sigma}(t,t') = i\left\langle a^\dagger_{n\boldsymbol{k}\sigma}(t')\, b_{\boldsymbol{k'}\sigma}(t)\right\rangle , \tag{37}$$

$$G^<_{\boldsymbol{k'}\sigma n\boldsymbol{k}}(t,t') = i\left\langle b^\dagger_{\boldsymbol{k'}\sigma}(t')\, a_{n\boldsymbol{k}\sigma}(t)\right\rangle . \tag{38}$$

© 2005 WILEY-VCH Verlag GmbH & Co. KGaA, Weinheim

In the formalism of the Keldysh nonequilibrium Green functions [20] we can express the lesser Green functions (37) and (38) by using the retarded (advanced) Green function $G_{r(a)}(E)$ for the interacting quantum well. Then the dc current can be expressed formally in a very compact form as follows

$$J_{\text{tot}} = \frac{(J_L^{\uparrow} - J_R^{\uparrow})}{2} + \frac{(J_L^{\downarrow} - J_R^{\downarrow})}{2} = \frac{e}{\hbar} \sum_{\sigma} \int \frac{\mathrm{d}E}{2\pi} T_{\sigma}(E)\,[f_L(E) - f_R(E)]\,. \tag{39}$$

Here the current J_R^{σ} through the right barrier has been calculated similarly to the left current in (36). The total "transmission coefficient" $T_{\sigma}(E)$in (39) is given by

$$T_{\sigma}(E) = \mathrm{Tr}\left\{\left(\frac{\Gamma_{\sigma}^{L}(E)\,\Gamma_{\sigma}^{R}(E)}{\Gamma_{\sigma}^{L}(E) + \Gamma_{\sigma}^{R}(E)}\right) i\,\frac{1}{2}\left[\boldsymbol{G}_r(E,\sigma) - \boldsymbol{G}_a(E,\sigma)\right]\right\} \tag{40}$$

where Γ and $\boldsymbol{G}$ are matrices in the quantum well indices *m, n*. The distribution function for the charge carriers in the left (right) lead is denoted by $f_{L(R)}(E)$. In deriving (40) we used (27) for the elastic coupling constants Γ_{σ}^{L} and Γ_{σ}^{R}, and we assumed that the coupling constants are proportional to each other, $\Gamma^{L} = \lambda\Gamma^{R}$.

In the case of the FQW the retarded (and advanced) Green function $G_{r(a)}$ needed in (40) is obtainable from the Dyson Eq. (30) and the self-energy (31):

$$G_{r(a)}(E_{nk\sigma}) = [E_{nk\sigma} - E_{nk\sigma}^{(1)} - \mathrm{Re}\{\Sigma_{\mathrm{SD}}^{\mathrm{2D}}(E_{nk\sigma})\} - \Sigma_{\Gamma}^{\mathrm{Re}}(E_{nk\sigma}) \pm i\gamma_{\sigma}(E_{nk\sigma})]^{-1} \tag{41}$$

where γ_{σ} includes the imaginary part of the self-energy (31) and the broadening of the energy levels caused by the finite life-time due to the tunneling processes:

$$\gamma_{\sigma}(E_{nk\sigma}) = \mathrm{Im}\,\{\Sigma_{\mathrm{SD}}^{\mathrm{2D}}(E_{nk\sigma})\} + \frac{\Gamma_{\sigma}}{2}\,. \tag{42}$$

Combining the results (27), (31), (39), (40) and (41) we can calculate the spin current through the FQW structures.

5 Charge carrier mobility in the FQW

To address the effects of the spin–spin interaction on the spin-dependent currents through the FQW from a fundamental point of view, we next study a simple system shown in Fig. 1, where a single resonant level with the energy $E_0^0(+\Sigma_{\Gamma}^{\mathrm{Re}})$ in the FQW is interacting with the magnetic lattice. For the ground state wave function we take a simple normalized trial function shown in Fig. 1(b):

$$\chi_0(y) = \left(\frac{\alpha}{2}\right)^{\frac{1}{2}} \mathrm{e}^{-\alpha|y|} \tag{43}$$

where α is the decay parameter. Furthermore, we take the wide band limit [34], i.e., we assume that the coupling coefficients $\Gamma^{L(R)}$ are independent of the energy. The perturbed energy levels in the FQW are obtainable from the poles of the retarded Green function (41). We have shown recently [33] in the case of the bulk magnetic semiconductors, that in the ferromagnetic region $T < T_{\mathrm{C}}$ the perturbed energy levels (band edges) are determined mainly by the first order correction (9), and that in the paramagnetic temperature region $T > T_{\mathrm{C}}$ there is a small, only slightly temperature dependent shift $\Delta_2 \approx -0.1\,\mathrm{eV}$ in the energy levels due to the higher order corrections. Therefore, based on the similarity between the 2D and

© 2005 WILEY-VCH Verlag GmbH & Co. KGaA, Weinheim

3D self-energies, Eqs. (31) and (33), we approximate the energy of the single resonant level in the FQW as follows

$$E_{\mathrm{res}}^{\sigma}(\boldsymbol{k}) = E_0^0 + \Sigma_{\Gamma}^{\mathrm{Re}} + \frac{\Delta_0^{(1)}}{2}(\delta_{\sigma\uparrow} - \delta_{\sigma\downarrow}) + \Delta_2 + \frac{\hbar^2}{2m^*}(k_x^2 + k_z^2) \tag{44}$$

where according to (10) and (43) the band splitting parameter reads

$$\Delta_0^{(1)} = -J_{\mathrm{exch}} x \left\langle S^Z \right\rangle F_0(W) \tag{45}$$

with

$$F_0(W) = \left(\frac{\alpha W}{2}\right) \sum_{|R_y| \le W/2} \mathrm{e}^{-2\alpha|R_y|}/N_y \,.$$

We can calculate the temperature and magnetic field dependent 2D mobility for the charge carriers inside the FQW in the case of the spin disorder scattering by estimating the scattering rate from the imaginary part of the self-energy (31):

$$\frac{1}{\tau_{\mathrm{SD}}^{\mathrm{2D}}(k_F\sigma)} = \frac{2\,\mathrm{Im}\,|\Sigma_{\mathrm{SD}}^{\mathrm{2D}}(k_F\sigma)|}{\hbar}$$

$$= \left(\frac{J_{\mathrm{exch}}^2}{8\pi\hbar}\right)[F_0(W)]^2 \int_0^{2\pi} \mathrm{d}\varphi \int_0^{\infty} \mathrm{d}q\, q \Big[C^{xx}\left(\sqrt{k_F^2 + q^2 - 2k_F q\cos\varphi}\right) F_L^{+}(q,\sigma)\,\delta_{\sigma\uparrow}$$

$$+ C^{yy}\left(\sqrt{k_F^2 + q^2 - 2k_F q\cos\varphi}\right) F_L^{-}(q,\sigma)\,\delta_{\sigma\downarrow} + C^{zz}\left(\sqrt{k_F^2 + q^2 - 2k_F q\cos\varphi}\right) F_L^{\pm}(q, \Delta_0^{(1)} = 0) \Big] \tag{46}$$

where

$$F_L^{\pm}(q,\sigma) = \frac{\Gamma/2}{\pi\left\{\frac{\Gamma^2}{4} + \left[\frac{\hbar^2}{2m^*}(k_F^2 - q^2) \pm \Delta_0^{(1)}\right]^2\right\}} \tag{47}$$

with $\Gamma = \Gamma^L + \Gamma^R$ and k_F is the Fermi-wave vector.

In deriving (46) we assumed that the width of the FQW is large enough so that the ferromagnetic subsystem behaves like a 3D ferromagnet, but still thin enough so that the position dependence of the spin correlation function $C(R_y) \sim \exp(-\kappa|R_y|)/|R_y|$ in the y-direction can be neglected, i.e., $\kappa|R_y| \ll 1$, when $|R_y| \le W/2$ and κ is the correlation length for the magnetic lattice. The former assumption is supported by the experimental observations [13] in (Ga,Mn)As, where the ferromagnetism remained even in 5–7 nm thin layers, which is a typical range of the widths for the III–V compound semiconductor quantum wells. Since [35] $\kappa \approx a_0^{-1}\sqrt{|T - T_{\mathrm{C}}|/T}$ and $W \approx 10a_0$ (a_0 = lattice constant), the condition $\kappa W/2 < 1$ is fulfilled at least at temperatures close to T_{C}, where the spin fluctuations and the spin disorder scattering rate (46) are largest. By assuming almost a constant spin correlation function in the y-direction we can perform the lattice summations over variables R_x and R_z, and finally obtain the result (46). The first two terms in (46) describe the spin-flip scattering events between the spin-up and spin-down states within the lowest subband of the FQW. Since we assume that in the FQW only a single resonant level exists, the transitions between the subbands are missing in (46).

© 2005 WILEY-VCH Verlag GmbH & Co. KGaA, Weinheim

The 2D scattering rate (46) can be compared with our previous result [26] for the 3D case, which is obtainable from (33):

$$\frac{1}{\tau_{\mathrm{SD}}^{\mathrm{3D}}(k_F\sigma)} = \frac{2\,\mathrm{Im}\,|\Sigma_{\mathrm{SD}}^{\mathrm{3D}}(k_F\sigma)|}{\hbar}$$

$$= \left(\frac{J_{\mathrm{exch}}^2 m^*}{8\pi\hbar^3}\right)\left\{\mathrm{Re}\sqrt{k_F^2 + \frac{2m^*\Delta_0^{(1)}}{\hbar^2}}\int_{-1}^{1} \mathrm{d}\xi\, C^{xx}[k_{1\sigma}(k_F,\xi,\Delta_0^{(1)})]\,\delta_{\sigma\uparrow}\right.$$

$$+\mathrm{Re}\left(\sqrt{k_F^2 - \frac{2m^*\Delta_0^{(1)}}{\hbar^2}}\right)\int_{-1}^{1} \mathrm{d}\xi\, C^{yy}[k_{1\sigma}(k_F,\xi,\Delta_0^{(1)})]\,\delta_{\sigma\downarrow}$$

$$\left. + k_F\int_{-1}^{1} \mathrm{d}\xi C^{zz}\left(\sqrt{2k_F^2 + 2k_F^2\xi}\right)\right\} \tag{48}$$

with

$$k_{1\sigma}(k_F,\xi,\Delta_0^{(1)}) = \mathrm{Re}\sqrt{2k_F^2 + \frac{2m^*\Delta_0^{(1)}}{\hbar^2}(\delta_{\sigma\uparrow} - \delta_{\sigma\downarrow}) + 2k\xi\,\mathrm{Re}\sqrt{k_F^2 + \frac{2m^*\Delta_0^{(1)}}{\hbar^2}(\delta_{\sigma\uparrow} - \delta_{\sigma\downarrow})}}\,. \tag{49}$$

In the 3D case the band splitting parameter $\Delta_0^{(1)}$ in (48) and (49) is calculated from (10) with $F_n(W) = 1$.

In the scattering rates (46) and (48) the Fourier transforms of the spin correlation functions (32) appear. They can be calculated in the molecular field approximation (MFA) by following and slightly modifying a procedure proposed by Sinkkonen [36]: In the MFA the average spin polarization of the magnetic moments is given by

$$\sum_{\boldsymbol{R}}\langle S_{\boldsymbol{R}}^z\rangle/N = x\langle S^z\rangle = xSB_S(\eta) = x\left(\frac{2S+1}{2}\right)\coth\left(\frac{2S+1}{2}\eta\right) - \frac{x}{2}\coth\left(\frac{\eta}{2S}\right) \tag{50}$$

where $N = N_x N_y N_z$ and S is the spin quantum number of the magnetic atoms (= 5/2 for Mn). $B_S(\eta)$ is the Brillouin function with

$$\eta = \frac{g_L\mu_{\mathrm{B}}S}{k_{\mathrm{B}}T}B_{\mathrm{eff}}\,. \tag{51}$$

The effective molecular field B_{eff} acting on the spin $\boldsymbol{S}_{\boldsymbol{R}}$ is obtained from the magnetic Hamiltonian (1):

$$B_{\mathrm{eff}} = B + \frac{2I(q=0)\langle S^z\rangle}{g_L\mu_{\mathrm{B}}}\,. \tag{52}$$

Here $I(q)$ is the Fourier transform of the ferromagnetic coupling parameter $I(\boldsymbol{R},\boldsymbol{R}')$ in (1), and in the case of the FCC lattice it is given by [37]

$$I(q) = \frac{3k_{\mathrm{B}}T_{\mathrm{C}}}{2S(S+1)}\left(1 - \frac{a_0^2 q^2}{12}\right). \tag{53}$$

© 2005 WILEY-VCH Verlag GmbH & Co. KGaA, Weinheim

When the spin correlation functions are calculated by using Sinkkonen's method, we have to take into account that a magnetic moment is found at a lattice site $\boldsymbol{R}$ with a probability x. Then we have

$$C^{xx}(q) = C^{yy}(q) = \frac{xS^2 B_S(\eta)/\eta}{1 - \dfrac{2S^2 I(q)\, B_S(\eta)/\eta}{k_B T}}$$

$$C^{zz}(q) = \frac{xS^2\, \partial B_S(\eta)/\partial\eta}{1 - \dfrac{2S^2 I(q)\, \partial B_S(\eta)/\partial\eta}{k_B T}}. \tag{54}$$

Figures 3 and 4 show the 2D and 3D mobilities vs. temperature as calculated from (46) and (48), respectively, with $\mu_{SD}^{2D(3D)}(T,\sigma) = e\tau_{SD}^{2D(3D)}(T,\sigma)/m^*$ in the cases, where the external magnetic field is either $B = 0$ T or 2 T. Here we have used the following material parameters valid for Mn-doped GaAs: $m^* = 0.5$ (a heavy hole band), $a_0 = 5.65$ Å, $T_C = 100$ K, $S = 5/2$, $x = 0.05$, Fermi wave vector $k_F = 10^9$ m^{-1} (in the 3D case this corresponds to a hole concentration $\approx 10^{19}$cm^{-3}), $\Gamma = 0.02$ eV [34], and $W = 10a_0$. The experimental values for the exchange parameter J_{exch} vary from 0.6 eV[12] to 3.3 eV [38]. Here we have chosen the larger value, which was obtained from the transport studies [38], and it leads to a value $J_{exch}F_0(W) = 1.2$ eV, when $\alpha W = 1.0$.

The Figs. 3 and 4 show, that the both mobilities μ_{SD}^{2D} and μ_{SD}^{3D} have a deep minimum at temperatures close to the Curie temperature, where the spin fluctuations and thereby the spin correlation functions are largest. Also one sees that the 3D mobility is smaller than the 2D mobility, which is what one expects, since in two dimensions the density of the final states to which the carriers can scatter is smaller and therefore the mobility is larger. However, when comparing these results one has to keep in mind, that in the 2D case the absolute value of μ_{SD}^{3D} depends on the detailed structure and geometry of the FQW, i.e., on the parameter αW. This is shown in Fig. 3, where the 2D mobility has been calculated for two different values of the wave function decay parameter α. The applied magnetic field reduces the spin fluctua-

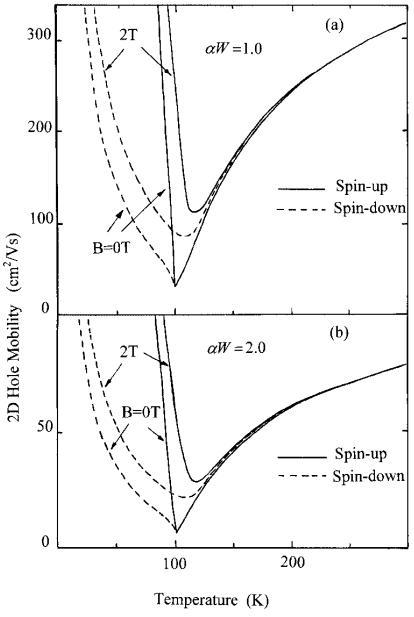

Fig. 3 Mobilities vs. temperature for the spin-up (solid curves) and spin-down (dashed curves) carriers in a two-dimensional charge carrier system (holes) inside an AlAs/GaMnAs/AlAs quantum well, when the external magnetic field is either zero or 2 T, and the wave function decay parameter α is (a) $\alpha W = 1.0$, or (b) $\alpha W = 2.0$, where W is the width of the quantum well. The values of the material parameters are given in the text.

© 2005 WILEY-VCH Verlag GmbH & Co. KGaA, Weinheim

Original
Paper

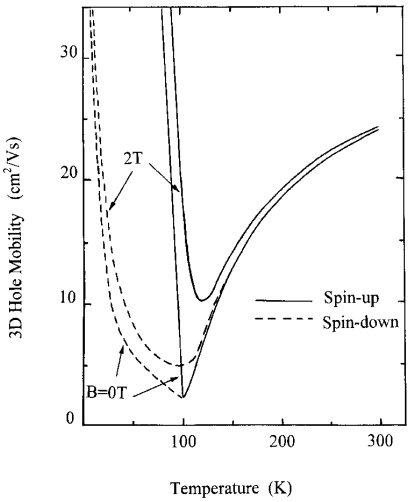

Fig. 4 Hole mobility vs. temperature in a bulk (3D) ferromagnetic semiconductor GaMnAs for spin-up (solid curves) and spin-down (dashed curves) carriers, when the external magnetic field is either zero or 2 T. The values of the material parameters are the same as in Fig. 3.

tions, and thereby the mobilities increase, as shown in Figs. 3 and 4. The minimum in mobility and the negative magnetoresistance have been observed experimentally in Mn-doped GaAs [38]. For the 2D hole gas there are no experimental mobility data yet. However, our calculated results shown in Fig. 3 indicate, that also in the 2D case the SD scattering may be the dominant scattering mechanism at temperatures close to T_C.

The SD scattering affects the spin transport through the FQW by broadening the resonant level according to (31) and (42). Therefore it is interesting to calculate the imaginary part of the self-energy (31) as a function of temperature and magnetic field from (46). As shown in Figs. 5 and 6, the applied mag-

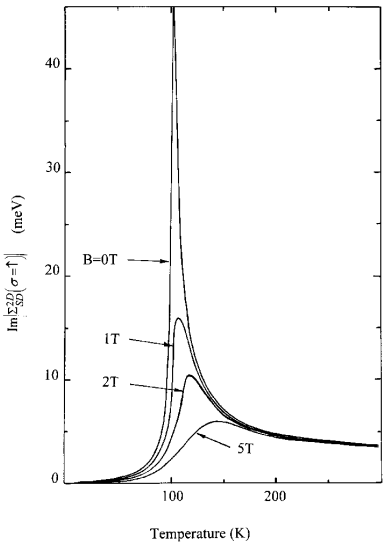

Fig. 5 Imaginary part of the self-energy (31) for spin-up carriers vs. temperature in various magnetic fields.

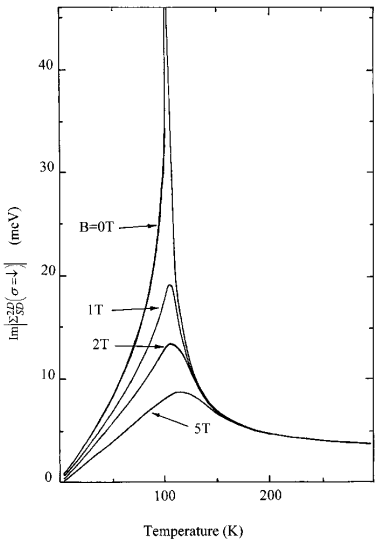

Fig. 6 Imaginary part of the self-energy (31) for spin-down carriers vs. temperature in various magnetic fields.

© 2005 WILEY-VCH Verlag GmbH & Co. KGaA, Weinheim

netic field reduces strongly $\mathrm{Im}\{\Sigma_{\mathrm{SD}}^{2\mathrm{D}}\}$ at temperatures close to T_{C}. Here we used the same material parameters as above in the case $\alpha W = 1.0$. By comparing the figures one sees that due to the band splitting effects in the ferromagnetic region, $\mathrm{Im}\{\Sigma_{\mathrm{SD}}^{2\mathrm{D}}\}$is larger for the spin-down carriers than for the spin-up carriers.

6 Spin dependent current through the FQW

Next we calculate the spin dependent current through the FQW structure shown in Fig. 1 by using the material parameters of $Ga_{1-x}Mn_xAs$ listed above. From (40) and (41) we get for the spin dependent transmission coefficient the following Lorenzian-type expression:

$$T_\sigma(E) = \left(\frac{\Gamma^L\Gamma^R}{\Gamma^L+\Gamma^R}\right)\frac{\gamma_\sigma^0}{(E-E_{\mathrm{res}}^\sigma)^2+\left[\frac{\gamma_\sigma^0}{2}\right]^2} \tag{55}$$

with

$$\frac{\gamma_\sigma}{2} = \mathrm{Im}\,|\Sigma_{\mathrm{SD}}^{2\mathrm{D}}(E_{\mathrm{res}}^\sigma)| + \frac{\Gamma^L+\Gamma^R}{2} \tag{56}$$

From (55) and (56) we see that due to the non-zero imaginary part of the self-energy (31) the exchange interaction broadens the transmission peak as compared to the non-interacting width $\Gamma/2$. In the limit $J_{\mathrm{exch}} \to 0$ (55) reduces to the non-interacting transmission coefficient derived previously by Wingreen et al. [34].

Figure 7 shows the calculated shift and the broadening of the total transmission coefficient $T_{\mathrm{tot}}(E) = \frac{1}{2}T_\uparrow(E) + \frac{1}{2}T_\downarrow(E)$ vs. energy at various temperatures, when the external magnetic field is zero. The results were calculated from (55) and (56) by using the following parameters for an AlAs/GaMnAs/AlAs quantum well: $E_0 + \Sigma_\Gamma^{\mathrm{Re}} = 0.2\,\mathrm{eV}$, $\Delta_2 = -0.08\,\mathrm{eV}$, $\alpha W = 1.0$ and $\Gamma = \Gamma^L + \Gamma^R = 0.02\,\mathrm{eV}$. In the ferromagnetic region $T < T_{\mathrm{C}} = 100$ K the spin−polarization of the resonant level, described by (9), is manifested in the transmission coefficient as an appearance of a double peak structure, so that the peak, which is lower in energy, corresponds to the spin-up resonant level and the upper peak to the spin-down

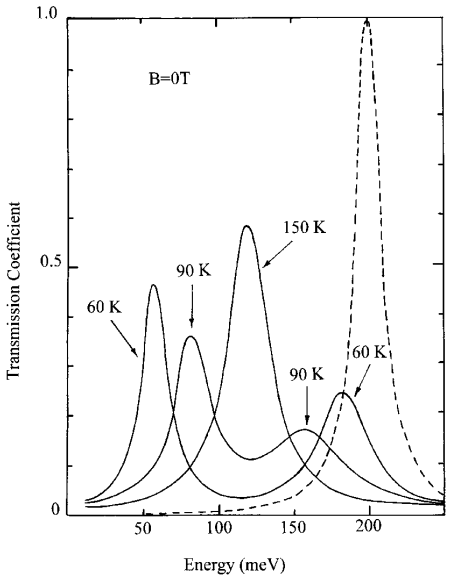

Fig. 7 Total transmission coefficient vs. incident energy for the carrier spins interacting with the ferromagnetic subsystem inside the FQW, when the external magnetic field is zero. The dashed curve shows the noninteracting ($J_{\mathrm{exch}} = 0$) transmission coefficient.

© 2005 WILEY-VCH Verlag GmbH & Co. KGaA, Weinheim

Original
Paper

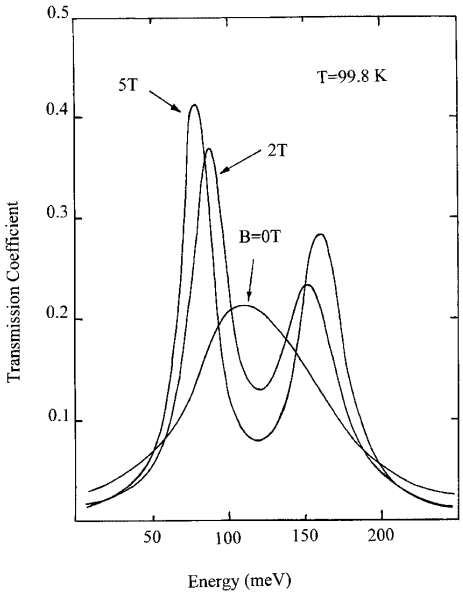

Fig. 8 Total transmission coefficient vs. incident energy for the carrier spins inside the FQW at $T = 99.8$ K ($T_C = 100$ K) in various external magnetic fields.

level. The same kind of broadening of $T_\sigma(E)$ as the one shown in Fig. 7 at $T > T_C$ has been observed in the case of the phonon scattering in nonmagnetic quantum wells [34]. The strong temperature dependence of $T_\sigma(E)$ in our model is a consequence of the temperature dependence of the average spin–polarization (2) and the spin correlation functions (54). Below T_C the peak in $T_\sigma(E)$ corresponding to the spin–down carriers is narrower than the peak corresponding to the spin-up carriers. This asymmetry is a consequence of the difference in the imaginary parts of the self-energies shown in Figs. 5 and 6. The results shown in Fig. 7 are similar to the theoretical results presented by Petukhov et al. [24] for (Ga,Mn)As RTDs. However, the strong temperature dependence of the peak widths shown in Fig. 7 is missing in the results of Ref. 24, since they neglected the effect of the SD scattering on the carrier lifetime in the FQW.

Figure 8 shows the total transmission coefficient vs. energy as calculated at a temperature 99.8 K, i.e., just below the Curie temperature 100 K. In zero magnetic field the small band splitting is shown only as a minor asymmetry in the $T_\sigma(E)$-curve. However, in higher magnetic fields the band splitting is manifested clearly as a double peak structure in the $T_\sigma(E)$-curve.

Figure 9 shows the dc current through the FQW structure vs. bias voltage at various temperatures, when the external magnetic field is zero. The results were calculated from (39) and (55) by assuming that the applied dc voltage V across the FQW structure is equally divided between the two barriers: $E_{res}(V) = E_{res}(\boldsymbol{k}) - eV/2$, where $E_{res}(\boldsymbol{k})$ is obtained from (44). Also the distribution function on the right hand side of the well was calculated from the one on the left hand side as $f_R(E) = f_L(E - eV)$. Since the current is proportional to the transmission coefficient in (39), it is obvious that the I–V characteristics reflect the same structure as $T_\sigma(E)$ vs. energy: due to the band splitting (9) the single peak in the current in the paramagnetic region splits into a double peak structure in the ferromagnetic region, as shown in Fig. 9.

Figure 10 shows the calculated dc current vs. bias voltage at $T = 99.8$ K in various magnetic fields. Also here the band splitting due to the applied magnetic field, is manifested as a double peak structure in the $I-V$ characteristics, just as in the transmission coefficient shown in Fig. 8. This is exactly the same behaviour, which has been found experimentally in the I–V characteristics of the AlAs/ErAs/AlAs quantum wells [16]. Recently Slobodskyy et al. [39] found the effect of a large Zeeman splitting on the I–V

© 2005 WILEY-VCH Verlag GmbH & Co. KGaA, Weinheim

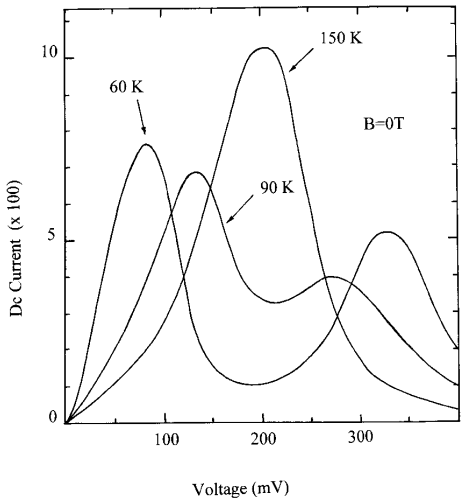

Fig. 9 Dc current through the FQW vs. bias voltage at various temperatures. The current is plotted in units of $e\Gamma/\hbar$.

characteristics of a paramagnetic ZnMnSe/ZnBeSe resonant tunneling diode, when they applied a high magnetic field to the RTD device. Their experimental results are in good agreement with our theoretical results shown in Fig. 10.

7 Conclusions

We have presented a quantum transport model for ferromagnetic resonant tunneling structures, where the quantized energy levels inside the quantum well, broadened by the tunneling processes, are strongly coupled to the ferromagnetic subsystem. An advantage of the chosen formalism is that only a single-particle retarded Green function must be solved for the quantum well region, and thereby the spin–spin interaction is included in the model in a straightforward manner. The magnetic ordering in the quantum

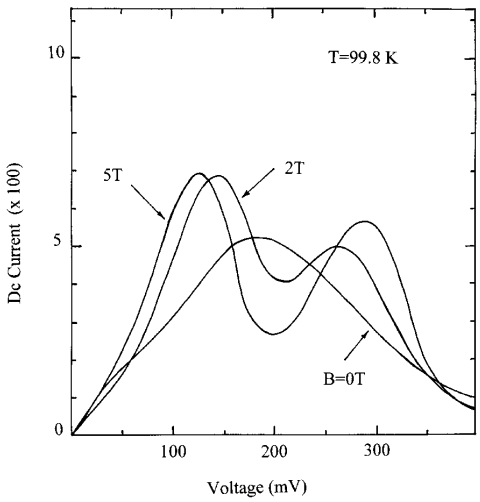

Fig. 10 Dc current through the FQW vs. bias voltage at $T = 99.8$ K in various external magnetic fields. The current is plotted in units of $e\Gamma/\hbar$.

© 2005 WILEY-VCH Verlag GmbH & Co. KGaA, Weinheim

well is manifested in the transmission coefficient $T(E)$ as strong temperature and magnetic field dependences. The splitting of the resonant level in a ferromagnetic quantum well is shown as a double peak structure in $T(E)$, and the strong spin disorder scattering broadens the peak significantly. The model can be improved by including a multi-band treatment, i.e., by taking into account the detailed structure of the valence band in the III–V ferromagnetic semiconductors (heavy and light holes and the spin–orbit split-off band). The transport theory presented here can be extended to other ferromagnetic mesoscopic devices such as magnetic quantum dots and wires or magnetic superlattices.

Acknowledgement This work has been supported by the Academy of Finland.

References

[1] S. Datta and B. Das, Appl. Phys. Lett. **56**, 665 (1990).
G. A. Prinz, Science **282**, 1660 (1998).
S. A. Wolf et al., Science **294**, 1488 (2001).
B. Kane, Nature (London) **393**, 133 (1998).
[2] D. D. Awschalom, N. Sarmarth, and D. Loss (Eds.), Semiconductor Spintronics and Quantum Computation, (Springer-Verlag, Berlin, 2002).
[3] H. Ohno and F. Matsukura, Solid State Commun. **117**, 179 (2001).
[4] I. Zutic, J. Fabian, and S. Das Sarma, Rev. Mod. Phys. **76**, 323 (2004).
[5] H. Ohno, H. Munekata, T. Penney, S. von Molnar, and L. L. Chang, Phys. Rev. Lett. **68**, 2664 (1992).
[6] H. Ohno, A. Shen, F. Matsukura, A. Oiwa, H. Endo, S. Katsumoto, and Y. Iys, Appl. Phys. Lett. **69**, 363 (1996).
[7] Y. Ohno, D. K. Young, B. Beshhoten, F. Matsukura, H. Ohno, and D. D. Awschalom, Nature (London) **402**, 790 (1999).
[8] Y. Ohno, I. Arata, F. Matsukura, K. Ohtami, S. Wang, and H. Ohno, Appl. Surf. Sci. **159–160**, 308 (2000).
[9] I. Arata, Y. Ohno, F. Matsukura, and H. Ohno, Physica E **10**, 288 (2001).
[10] T. Hayshi, M. Tanaka, K. Seto, and T. Nishinaga, J. Appl. Phys. **83**, 6551 (1998).
[11] D. Chiba, N. Akiba, F. Matsukura, Y. Ohno, and H. Ohno, Appl. Phys. Lett. **77**, 1873 (2000).
[12] H. Ohno, N. Akiba, F. Matsukura, A. Shen, K. Ohtani, and Y. Ohno, Appl. Phys. Lett. **73**, 363 (1998).
[13] T. Hayashi, M. Tanaka, K. Seto, and T. Nishinaga, Appl. Phys. Lett. **71**, 1825 (1997).
[14] R. Tsu and L. Esaki, Appl. Phys. Lett. **22**, 562 (1973).
[15] H. Mizuta and T. Tanone, The Physics and Applications of Resonant Tunnelling Diodes (Cambridge University Press, Cambridge, 1995).
[16] D. E. Brehmer, K. Zhang, C. J. Schwarz, S.-P. Chau, S. J. Allen, J. P. Ibbetson, J. P. Zhang, C. J. Palmstrom, and B. Wilkins, Appl. Phys. Lett. **67**, 1268 (1995).
[17] A. Haury, A. Wasiela, A. Arnoult, J. Cibert, S. Tatarenko, T. Dietl, and Y. Merle d'Aubigne, Phys. Rev. Lett. **79**, 511 (1997).
[18] D. K. Ferry and S. M. Goodnick, Transport in Nanostructures (Cambridge University Press, Cambridge, 1997).
[19] Y. Meir and N. S. Wingreen, Phys. Rev. Lett. **68**, 2512 (1992).
[20] A.-P. Jauho, N. S. Wingreen, and Y. Meir, Phys. Rev. B **50**, 5528 (1994).
[21] H. Haug and A.-P. Jauho, Quantum Kinetics in Transport and Optics of Semiconductors (Springer-Verlag, Berlin, 1998).
[22] S. Nonoyama and J. Inoue, Physica E **10**, 283 (2001).
[23] A. G. Petukhov, A. N. Chantis, and D. O. Demchenko, Phys. Rev. Lett. **89**, 107205 (2002).
[24] A. G. Petukhov, D. O. Demchenko, and A. N. Chantis, J. Vac. Sci. Technol. B **18**, 2109 (2000).
[25] A. G. Petukhov, D. O. Demchenko, and A. N. Chantis, Phys. Rev. B **68**, 125332 (2003).
[26] N. Lebedeva and P. Kuivalainen, J. Appl. Phys. **93**, 9845 (2003).
[27] J. Fabian, I. Zutic, and S. Das Sarma, Phys. Rev. B **66**, 165301 (2002).
[28] I. Zutic, J. Fabian, and S. Das Sarma, Phys. Rev. Lett. **88**, 066603 (2002).
[29] J. Fabian, I. Zutic, and S. Das Sarma, Appl. Phys. Lett. **84**, 85 (2004).
[30] J. Fabian and I. Zutic, Phys. Rev. B **69**, 115314 (2004).
[31] D. N. Zubarev, Nonequilibrium Statistical Thermodynamics (Consultant Bureau, New York, 1974).
[32] R. M. White, Quantum Theory of Magnetism (McGraw-Hill, New York, 1971).

© 2005 WILEY-VCH Verlag GmbH & Co. KGaA, Weinheim

[33] N. Lebedeva and P. Kuivalainen, J. Phys.: Condens. Matter **14**, 4491 (2002).
[34] N. S. Wingreen, K. W. Jacobsen, and J. W. Wilkins, Phys. Rev. B **40**, 11834 (1989).
[35] R. J. Elliot and W. Marshall, Rev. Mod. Phys. **30**, 75 (1958).
[36] J. Sinkkonen, Phys. Rev. B **23**, 6638 (1980).
[37] K. Kaski, J. Sinkkonen, P. Kuivalainen, and T. Stubb, J. Phys. C: Solid State Phys. **13**, 5233 (1980).
[38] F. Matsukura, H. Ohno, A. Shen, and Y. Sugawara, Phys. Rev. B **57**, R2037 (1998).
[39] A. Slobodskyy, C. Gloud, T. Slobodskyy, C. R. Becker, G. Schmidt, and L .W. Molenkamp, Phys. Rev. Lett. **90**, 246601 (2003).

© 2005 WILEY-VCH Verlag GmbH & Co. KGaA, Weinheim